Chemical Engineering Journal 308 (2017) 222–228

Contents lists available at ScienceDirect

Chemical Engineering Journal

journal homepage: www.elsevier.com/locate/cej

Free standing three-dimensional nitrogen-doped carbon nanowire array for high-performance supercapacitors

Guiyin Xu [a,b], Hui Dou [a,*], Xiumei Geng [b], Jinpeng Han [a], Lifeng Chen [c], Hongli Zhu [b,*]

[a] Jiangsu Key Laboratory of Material and Technology for Energy Conversion, College of Material Science and Engineering, Nanjing University of Aeronautics and Astronautics, Nanjing 210016, PR China
[b] Department of Mechanical and Industrial Engineering, Northeastern University, Boston, MA 02115, USA
[c] Department of Chemistry, Chemistry Experiment Teaching Center, University of Science and Technology of China, Hefei, Anhui 230026, PR China

HIGHLIGHTS

- Three-dimensional ACNTP/NC nanowire arrays were obtained by a facial process.
- Nitrogen doping increases the specific capacitance by a pseudocapacitive effect.
- The ACNTP/NC electrode exhibit excellent electrochemical performance.

GRAPHICAL ABSTRACT

Three-dimensional nitrogen-doped carbon nanowire arrays show excellent electrochemical performance for supercapacitors.

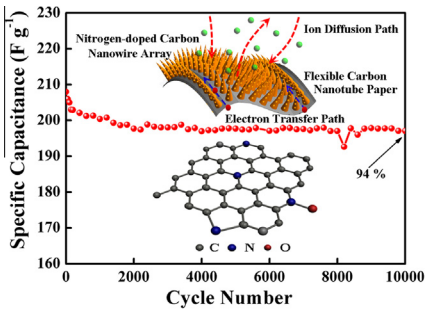

ARTICLE INFO

Article history:
Received 20 July 2016
Received in revised form 25 August 2016
Accepted 12 September 2016
Available online 12 September 2016

Keywords:
Polyaniline
Free standing
Carbon nanotube paper
Nitrogen-doped carbon nanowire
Supercapacitors

ABSTRACT

Three-dimensional polyaniline nanowire arrays are vertically grown on free-standing acidized carbon nanotube paper, and further carbonized to nitrogen doped carbon for supercapacitor electrodes. The three-dimensional porous structure of the as-prepared nitrogen doped carbon can increase the specific surface area and benefit ion transport into the interior of the electrode materials. Nitrogen doping can effectively improve the wettability of the carbon surface in the electrolyte and enhance the specific capacitance by a pseudocapacitive effect. Thus, free-standing nitrogen doped carbon nanowires on conductive carbon nanotube paper show excellent electrochemical performance as a supercapacitor electrode material. At a current density of 2 A g^{-1}, the specific capacitance reaches 210 F g^{-1} with 94% capacitance retention after 10,000 cycles.

1. Introduction

Electrochemical energy storage systems, including lithium ion batteries and supercapacitors, have been paid much attention due to their environmental friendliness, sustainability, and stability [1–5]. Supercapcitors especially have high power density to allow for the development of fast and high-power electronic devices [6–10]. The main electrode materials for supercapacitors are metal oxides, electrically conducting polymers, and carbon materials [11]. Supercapacitors based on conductive metal oxides show high specific capacitance and excellent rate capability [12]. However, conductive metal oxides such as RuO_2 are toxic and expensive, preventing widespread application in supercapacitors. Other relatively low-cost metal oxides, including Co_3O_4 and MnO_2, have poor electrical conductivity and thus exhibit poor

* Corresponding authors.
E-mail addresses: dh_msc@nuaa.edu.cn (H. Dou), h.zhu@neu.edu (H. Zhu).

http://dx.doi.org/10.1016/j.cej.2016.09.060
1385-8947/

electrochemical performance at high current densities [13–15]. Conducting polymers, such as polyaniline, polythiophene and polypyrrole, have high specific capacitance, energy density and power density [16–18]. These electroactive polymers, however, suffer from swelling, shrinking and degradation during the charge/discharge process, leading to poor cycling stability. Carbon-based supercapacitors, also referred to as electrochemical double layer capacitors, have potential application prospects in the field of portable electronic devices, advanced electric vehicles, and unmanned aerial vehicle due to their low-cost, high power density, and long cycle life [19–22].

Low energy density hampers the development and practical application of carbon supercapacitors for large-scale electronic equipment [23–26]. There are two main approaches to increase the energy density according to $E = 0.5CV^2$ [27,28]. One method is to increase the operating voltage window of supercapacitors. For example, the use of organic or ionic liquid electrolytes in supercapacitors can greatly increase the voltage window [29,30]. Phosphorus-doped carbon materials as electrode materials of supercapacitors have relatively better stability in aqueous solutions, resulting in a wider potential window compared with that of carbon materials [31,32]. The other method is to improve the specific capacitance of supercapacitors by designing electrode materials with high specific surface area, optimized microstructure, unique pore size distribution, and excellent electric conductivity [11,33–36].

Recently, nitrogen-doped carbon materials have received extensive attention because of their good electrochemical performance owing to good wettability with aqueous electrolytes and enhanced specific capacitance from additional pseudocapacitance [37–40] and [40]. One-dimensional (1D) nitrogen-doped carbon nanotubes [41] and nanofibers [42], two-dimensional (2D) nitrogen-doped graphene [43], and three-dimensional (3D) nitrogen-doped porous carbon [44] have been widely investigated for supercapacitors. The 3D nitrogen-doped porous carbons especially show excellent electrochemical performance due to sufficient electrolyte infiltration and shorter ion diffusion lengths [38,45,46]. However, the binder material commonly required in the preparation of nitrogen-doped carbon electrodes for supercapacitors does not contribute to the specific capacitance and therefore reduces the energy density. As such it is desirable to design binder-free nitrogen-doped carbon materials to improve the energy density.

Herein, we demonstrate a nitrogen-doped carbon nanowire array on flexible carbon nanotube paper as a 3D electrode material for supercapacitors. In the synthesis, aniline (ANI) is polymerized to a vertical polyaniline (PANI) nanowire array on acidized carbon nanotube paper (ACNTP) to obtain an acidized carbon nanotube paper/polyaniline (ACNTP/PANI) composite. Then, the ACNTP/PANI is carbonized under nitrogen to form the acidized carbon nanotube paper/nitrogen-doped carbon (ACNTP/NC) electrode. The nitrogen-doped carbon nanowire array is vertically grown on ACNTP resulting in a 3D nanostructure, which increases the specific surface area and provides ion diffusion channels. In this way, the specific capacitance and rate performance of ACNTP/NC are enhanced. Therefore, ACNTP/NC as a free-standing electrode material for supercapacitors has great potential in increasing the rate performance and energy density.

2. Experimental section

2.1. Preparation of ACNTP/PANI and ACNTP/NC

Carbon nanotube paper (CNTP) was obtained from Suzhou Jiedi Nano Science and Technology Co. Ltd. in China and punched into squares (2 * 2 cm). Then, the CNTP squares were treated by backflow in 6 M HNO_3 aqueous solution at 100 °C for 8 h. The resulting acidized carbon nanotube paper (ACNTP) was repeatedly washed with water and pure ethanol. Finally, the ACNTP was dried at 60 °C for 12 h.

The ACNTP square and 0.02 M aniline monomer were added into 30 mL of 1 M HCl and stirred for 6 h at 4 °C. $(NH_4)_2S_2O_8$ (APS) was dissolved in 20 mL of 1 M HCl (the molar ratio of aniline/APS is 1:1) and dropwise added into the above HCl solution. The mixture was stirred for 6 h at 4 °C. The prepared material is named ACNTP/PANI-2 and repeatedly washed with water and dried at 60 °C for 12 h. All other conditions equal, the amount of aniline monomer and APS were varied to prepare similar samples. These materials are named ACNTP/PANI-1 and ACNTP/PANI-3, corresponding to aniline monomer concentration of 0.01 M and 0.04 M, respectively.

The obtained ACNTP/PANI was transferred to a tube furnace and heat-treated at 700 °C for 2 h under nitrogen with a heating rate of 5 °C min^{-1}. Then, the as-prepared sample was cooled to room temperature and ACNTP/NC-1, ACNTP/NC-2, and ACNTP/NC-3 correspond to ACNTP/PANI-1, ACNTP/PANI-2 and ACNTP/PANI-3, respectively.

2.2. Characterization

Fourier transform infrared spectroscopy (FTIR) measurements were recorded on a Nicolet 750. Field emission scanning electron microscopy (FESEM) was carried out with JEOL JSM-6380LV FE-SEM. The X-ray photoelectron spectroscopy (XPS) analysis was performed on a Perkin-Elmer PHI 550 spectrometer with Al Kα (1486.6 eV) as the X-ray source. The Raman spectra of ACNTP and ACNTP/NC were measured by using a Jobin Yvon HR800 confocal Raman system with a 632.8 nm diode laser excitation on a 300 line S mm^{-1} grating at room temperature. The N_2 adsorption/desorption tests were determined by Brunauer-Emmett-Teller (BET) measurements using an ASAP-2010 surface area analyzer. The pore size distribution (PSD) was derived from the desorption branch of the isotherm with the Barrett-Joyner-Halenda (BJH) method.

2.3. Electrochemical characterization

To measure the electrochemical properties of ACNTP/PANI, 5 mg of active material was put on stainless steel grids. The electrodes were assembled together with 1 M H_2SO_4 aqueous electrolyte solution. For the ACNTP/NC electrodes, the 5 mg active material was put onto foamed Ni grids and a 6 M KOH aqueous solution was used for the electrolyte. These electrodes were dried at 60 °C for several hours before pressing under a pressure of 15 MPa. Cyclic voltammetry (CV) and galvanostatic charge/discharge experiments were performed on a CHI 660A electrochemical workstation (Shanghai Chenhua, China) in a conventional three-electrode system. Platinum foil and a saturated calomel electrode (SCE) were used as counter and reference electrodes. The specific capacitances are calculated from the galvanostatic charge/discharge curves based on the following equation:

$$C = \frac{It}{m\Delta V}$$

where C, I, t, m and ΔV are the specific capacitance (F g^{-1}), the discharging current (A), the discharging time (s), the mass of active material (g) and the discharging potential range (V), respectively. Electrochemical impedance spectroscopy (EIS) was measured in the frequency range of 100 kHz–10 mHz with an amplitude of 5 mV.

3. Results and discussion

Carbon nanotube paper (CNTP) is a promising flexible substrate due to its excellent electrical conductivity and mechanical properties [47,48]. To introduce the negatively charged groups on the surface of CNTP, the CNTP was treated by nitric acid acidification. This process allows for the introduction of oxygen-rich functional groups including hydroxyl (O—H) and carboxyl (—COOH) groups (Fig. S1). These negatively charged groups can be used as nucleation sites for aniline groups on the surface of ACNTP (Fig. 1a). The absorption bands at 1580 and 1480 cm^{-1} correspond to the vibrations of the quinoid and benzenoid ring of PANI in the FTIR spectrum of ACNTP/PANI [49], demonstrating that PANI is successfully loaded on ACNTP (Fig. S1). Additionally, the acid treatment process has no effect on the flexibility and microstructure of ACNTP (Fig. S2). The PANI nanowire array then undergoes a carbonization process under nitrogen to form a nitrogen-doped carbon nanowire array. A porous structure is formed in ACNTP/NC during the carbonization process when H_2O, CO_2 and CO are evaporated from the PANI nanowire array. This process can increase the specific surface area and pore volume (Fig. 1b). The carbon nanowire array and ACNTP constitute the 3D structure with improved ion diffusion. The ACNTP provides high electrical conductivity, increasing the active material utilization and electrochemical performance. The nitrogen doping can be verified by the absorption band at 1460 cm^{-1} corresponding to the C-N stretching vibration in the FTIR spectrum of ACNTP/NC (Fig. S1) [49,50].

Morphology characterization is performed to confirm the predicted nanostructure. Uniform PANI nanowires on ACNTP were obtained by optimizing the concentration of aniline in the preparation process. Aniline monomers tend to exhibit heterogeneous nucleation on the surface of the substrate at low concentration and form aligned polyaniline nanowires according to the nucleation mechanism of polyaniline [51]. However, homogeneous nucleation in solution can form randomly connected polyaniline nanowires and heterogeneous nucleation generates aligned polyaniline nanowires on the substrate at high concentration. When the concentration of aniline monomer is 0.02 M, a PANI nanowire array uniformly covers the ACNTP to form ACNTP/PANI-2 (Fig. 2a, b). When the concentration of aniline monomer decreases to 0.01 M, the PANI nanowires inhomogenously distribute on ACNTP, resulting in the presence of some incompletely covered carbon nanotubes in ACNTP/PANI-1. (Fig. S3a). When the aniline monomer concentration increases to 0.04 M, some randomly connected polyaniline nanowires from the solution deposit onto the substrate for ACNTP/PANI-3 in addition to the PANI nanowire array (Fig. S3b). The arrangement of the PANI nanowires is maintained during the high temperature carbonization process. The nitrogen-doped carbon nanowire arrays are homogenously distributed on the substrate for ACNTP/NC-2 (Fig. 2c, d). However, there is no uniform carbon array in ACNTP/NC-1 (Fig. S3c). The random carbon accumulation of ACNTP/NC-3 impedes ion diffusion and reduces the utilization ratio of electrode materials (Fig. S3d).

ACNTP/NC-2 is composed of carbon, nitrogen and oxygen according to the XPS survey (Fig. 3a). In the C 1s spectra of ACNTP/NC-2, the peaks at 289.2, 287.3, 285.6 and 284.7 eV are attributed to O—C=O, C=O, C—O and C—C bonds (Fig. 3b), respectively [52,53]. In the nitrogen spectra of ACNTP/NC-2, the peaks at 403.2, 400.8, 399.9 and 398.5 eV are associated with oxidized nitrogen (N1), quaternary nitrogen (N2), pyrrolic nitrogen (N3), and pyridinic nitrogen (N4) (Fig. 3c) [42]. In the O 1s spectra of

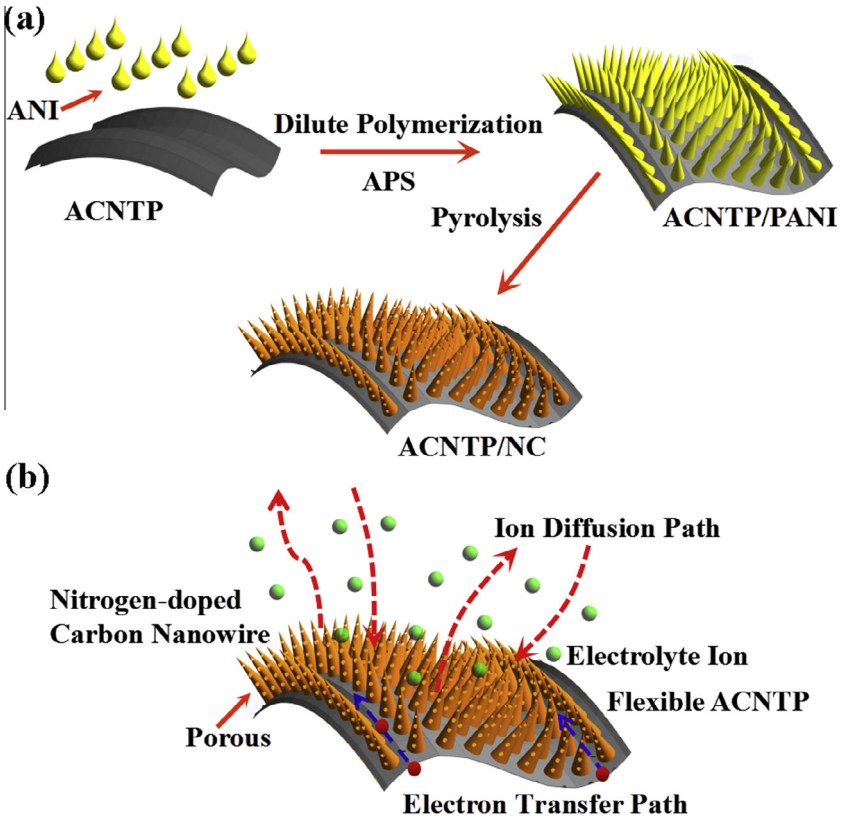

Fig. 1. Schematic illustration for (a) the preparation and (b) electrochemical process of the ACNTP/NC composite. The preparation process mainly includes polymerization and pyrolysis. The green dots in (b) represent electrolyte ions. The red dots indicate electrons. The binder free free-standing 3D porous nitrogen doped carbon provides both efficient electron transfer path and ion diffusion surfaces. (For interpretation of the references to color in this figure legend, the reader is referred to the web version of this article.)

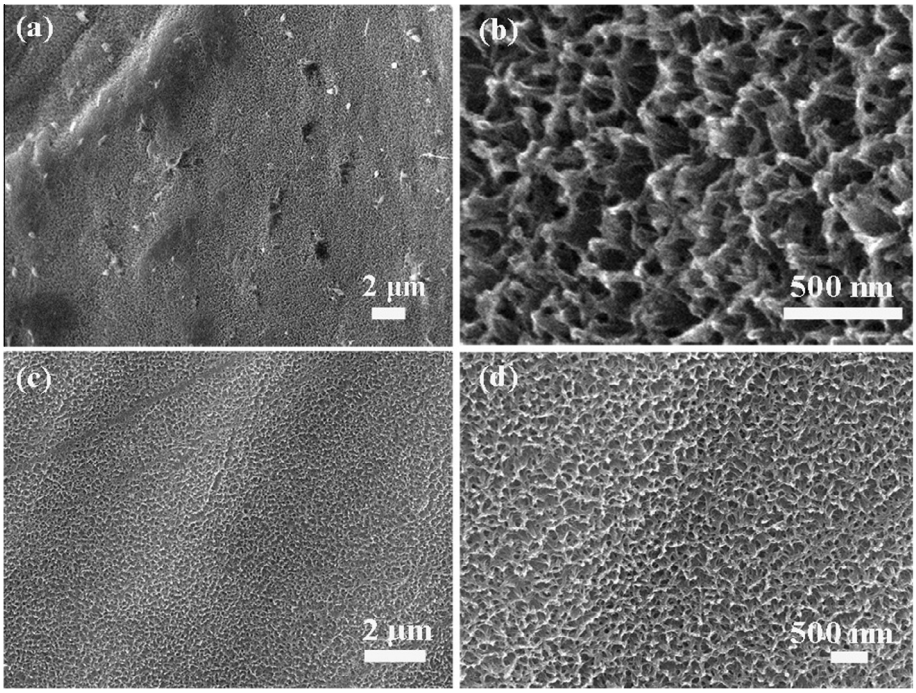

Fig. 2. Scanning electron microscopy (SEM) images of (a, b) ACNTP/PANI-2 and (c, d) ACNTP/NC-2. Polyaniline and nitrogen-doped carbon nanowire arrays are grown on ACNTP and thus constitute the 3D porous structure.

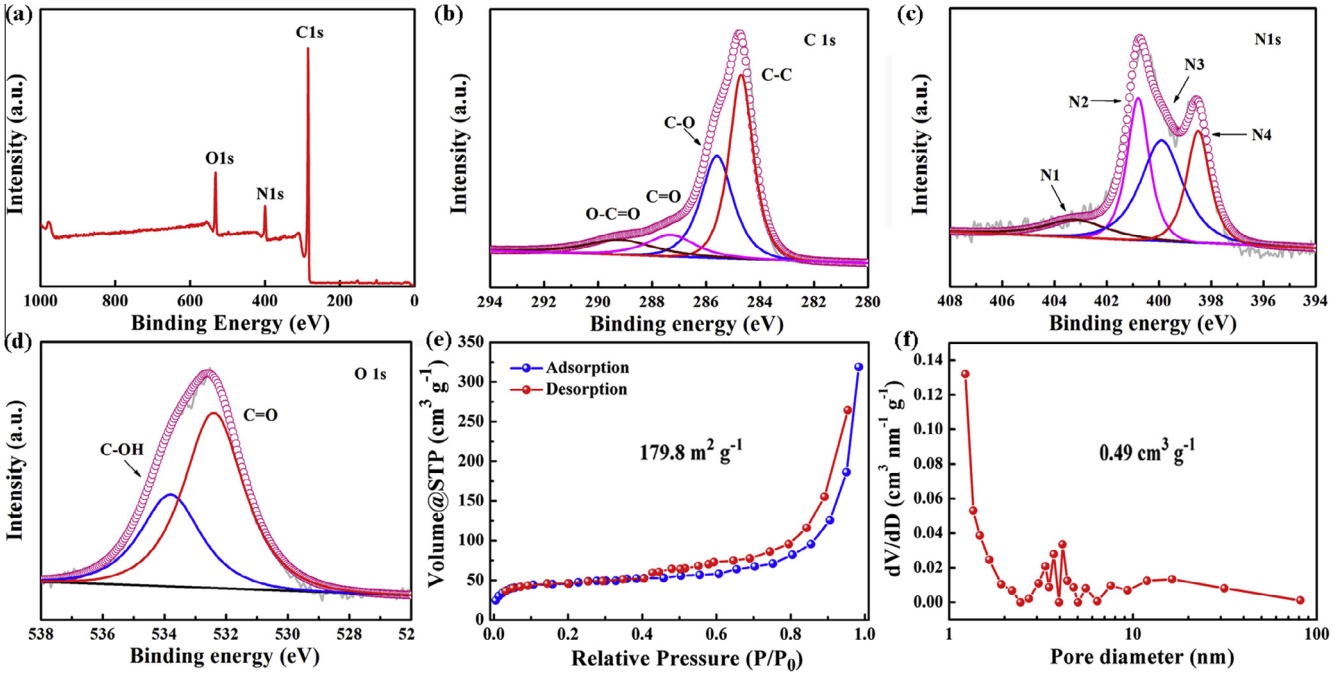

Fig. 3. (a) XPS survey and (b) C 1s, (c) N 1s, (d) O 1s XPS spectra for ACNTP/NC-2. (e) N_2 adsorption/desorption isotherms at 77 K and (f) pore size distribution (PSD) curve of ACNTP/NC-2. The nitrogen-doped carbon nanowire, carbon nanotube paper, and the 3D porous structure contribute to the specific surface area of 179.8 $m^2\ g^{-1}$ and pore volume of 0.49 $cm^3\ g^{-1}$.

ACNTP/NC-2, the peaks at 533.8 and 532.4 eV correspond to C═O and C—OH bonds (Fig. 3d), respectively [54]. Similar results for the carbon, nitrogen, and oxygen bonding in ACNTP/NC-1 and ACNTP/NC-3 are shown in Fig. S4. ACNTP/NC-2 has a high nitrogen content of 8.43% compared to 5.21% in ACNTP/NC-1 and 7.55% in ACNTP/NC-3 (Table S1). The specific surface area of ACNTP/NC-2 is 179.8 $m^2\ g^{-1}$, while for ACNTP/NC-1 and ACNTP/NC-3 it is 58.2 $m^2\ g^{-1}$ (Fig. S5b) and 87.7 $m^2\ g^{-1}$ (Fig. S5c), respectively. The presence of micropores and mesopores in ACNTP/NC-2 is indicated from an uptrend at low relative pressure ($P/P_0 < 0.1$) and the hysteresis characteristics at the high relative pressure ($P/P_0 = 0.4–0.95$) in the isotherms (Fig. 3e). ACNTP/NC-2 has a pore volume of 0.49 $cm^3\ g^{-1}$, which is larger than 0.42 $cm^3\ g^{-1}$ of ACNTP/NC-1 and 0.47 $cm^3\ g^{-1}$ of ACNTP/NC-3. An uptrend at

~1 nm in the PSD curve of ACNTP/NC-2 also indicates the presence of rich micropores (Fig. 3f). These abundant micropores are ideal for ion diffusion, thus increasing the electrochemical performance. The primary pore diameter is ~6 nm in ACNTP/NC-1 (Fig. S5e) and ~2.5 nm in ACNTP/NC-3 (Fig. S5f).

Fig. 4a displays the CV results of the ACNTP/PANI-2 based supercapacitors. Two pairs of redox peaks are observed, consistent with known redox transitions in PANI [51]. The ACNTP/PANI-2 has a specific capacitance of 307 F g^{-1} at a current density of 1 A g^{-1} (Fig. 4b). The galvanostatic charge/discharge curves of the ACNTP/PANI-2 electrode show a slight bend; a result of the pseudocapacitive effect. The specific capacitances of ACNTP/PANI-1 and ACNTP/PANI-3 are 229 and 285 g^{-1} at a current density of 1 A g^{-1} (Fig. 4c). Increasing the current density to 20 A g^{-1} yields specific capacitances of 145, 204, and 186 F g^{-1} for ACNTP/PANI-1, ACNTP/PANI-2 and ACNTP/PANI-3 respectively. Meanwhile, the capacitance retention rate of ACNTP/PANI-2 (66.4%) is higher than that of ACNTP/PANI-1 (63.3%) and ACNTP/PANI-3 (65.3%). ACNTP/PANI-2 exhibits the best rate performance and retained specific capacitance owing to the synergistic effect of highly conductive ACNTP and well-ordered PANI nanowires.

The CV results for ACNTP/NC-2 exhibit the regular rectangular shapes at low scan rates and maintain an approximately rectangular shape at a high scan rate of 500 mV s^{-1} (Fig. 4d), indicating fast electron and ion transport in the ACNTP/NC-2 electrode. The galvanostatic charge/discharge curves of the ACNTP/NC-2 electrode exhibit a small deviation from linearity (Fig. 4e), which is attributed to a pseudocapacitive effect from the nitrogen doping. ACNTP/NC-2 shows a high specific capacitance of 210.4 F g^{-1} at a current density of 2 A g^{-1} in comparison with previous reports (Table S2). ACNTP/NC-1 and ACNTP/NC-3 also exhibit good specific capacitances of 80 and 118 F g^{-1} at the same current density due to the high content nitrogen doping (Fig. 4f). The specific capacitance of ACNTP/NC-1, ACNTP/NC-2 and ACNTP/NC-3 decrease to 38.6, 126.7 and 47.8 F g^{-1} at a high current density of 50 A g^{-1}. The capacitance retention rate of ACNTP/NC-2 is 60.2%; higher than that of ACNTP/NC-1 (48.3%) and ACNTP/NC-3 (40.5%). Additionally, the capacitance retention rate of the ACNTP/NC-2 electrode is up to 94% after 10,000 cycles (Fig. S7), demonstrating that the ACNTP/NC-2 electrodes have a stable long term performance. The unique nanostructure of ACNTP/CN-2 facilitates fast ion diffusion and allows the electrolyte to fully infiltrate into the interior of the electrode materials (Fig. S8), resulting in enhanced electrochemical performance.

4. Conclusions

In summary, the microstructures of the polyaniline nanowire array/acidized carbon nanotube paper composite and nitrogen-doped carbon/acidized carbon nanotube paper composite were optimized by controlling the concentration of aniline. The precursor ACNTP/PANI-2 shows a high specific capacitance of 307 F g^{-1} at a current density of 1 A g^{-1}, which results from the unique 3D structure and the synergistic effect of the highly conductive ACNTP and well-ordered PANI nanowires. After the carbonization of ACNTP/PANI-2, the 3D structure and nitrogen doping in the ACNTP/NC-2 nanocomposite promotes ion transport and electrolyte infiltration. Moreover, nitrogen doping improves specific capacitance by the pseudocapacitive effect. Thus, the free-standing ACNTP/NC-2 should exhibit excellent electrochemical performance. The specific capacitance of ACNTP/NC-2 reaches 210.4 F g^{-1} at a current density of 2 A g^{-1}. Additionally, the capacitance retention reaches 94% after 10,000 cycles at the same current density. Even at a high current density of 50 A g^{-1}, ACNTP/NC-2 retains a high specific capacitance of 126.7 F g^{-1}, demonstrating the excellent rate performance. Based on the outstanding electrochemical performance in this work, the free-standing ACNTP/NC-2 with nitrogen doping is a promising catalyst material for photocatalysis and electrode material for lithium-air and lithium-sulfur batteries.

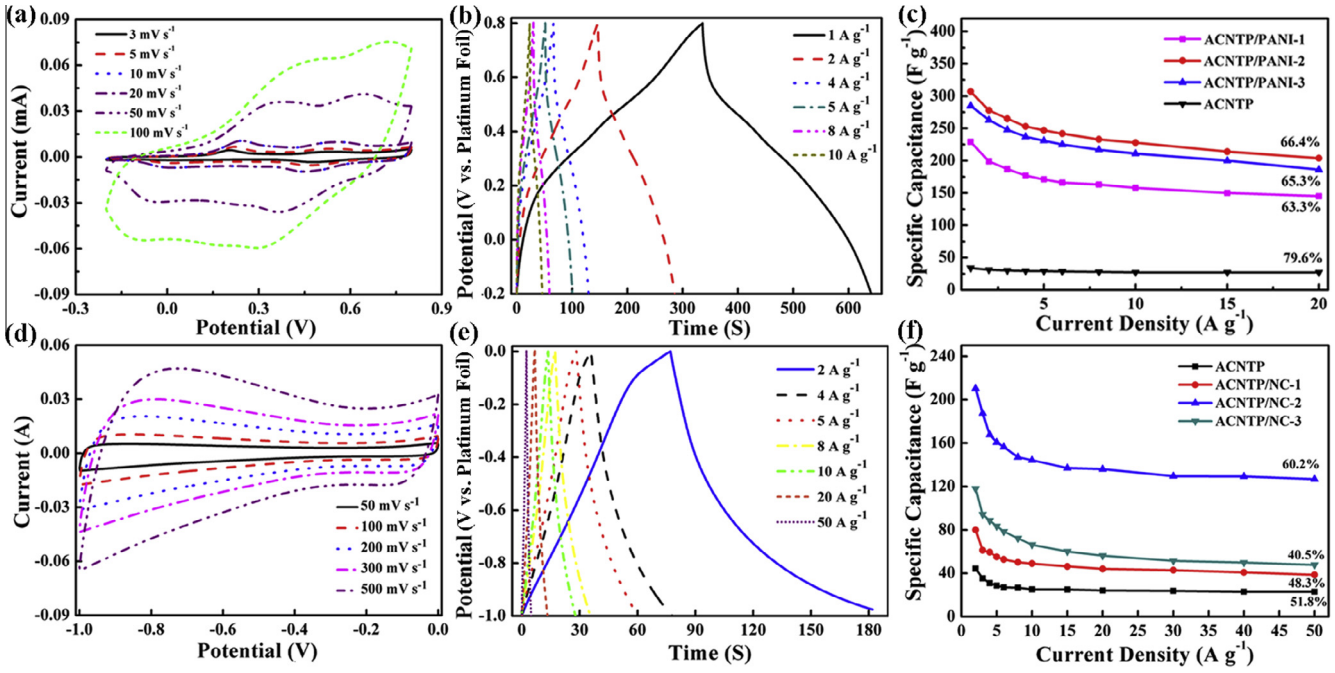

Fig. 4. (a) Cyclic voltammetry (CV) curves of the ACNTP/PANI-2 electrode in 1 M H_2SO_4 at different scan rates. (b) The galvanostatic charge/discharge curves of the ACNTP/PANI-2 electrode at different current densities. (c) The specific capacitances of ACNTP and ACNTP/PANI electrodes under different current densities. (d) CV curves of the ACNTP/NC-2 electrode in 6 M KOH at different scan rates. (e) The galvanostatic charge/discharge curves of the ACNTP/NC-2 electrode at different current densities. (f) The specific capacitances of ACNTP and ACNTP/NC electrodes under different current densities.

Acknowledgements

G.Y. Xu and H. Dou contributed equally to this work. The authors are grateful to the National Key Basic Research Program 973 (No. 2014CB239701), National Natural Science Foundation of China (No. 51372116, 21503207), Natural Science Foundation of Jiangsu Province (No. BK20151468, BK2011030, BK2011740), Fundamental Research Funds for the Central Universities of NUAA (NJ20160104) and A Project Funded by the Priority Academic Program Development of Jiangsu Higher Education Institutions (PAPD). H.L. Zhu acknowledges the startup support from Northeastern University. G.Y. Xu would like to thank Funding of Jiangsu Innovation Program for Graduate Education (KYLX15_0300) and Outstanding Doctoral Dissertation in NUAA (BCXJ15-07).

Appendix A. Supplementary data

Supplementary data associated with this article can be found, in the online version, at http://dx.doi.org/10.1016/j.cej.2016.09.060.

References

[1] J.W. Choi, D. Aurbach, Promise and reality of post-lithium-ion batteries with high energy densities, Nat. Rev. Mater. 1 (2016) 16013.
[2] W. Bao, J. Wan, X. Han, X. Cai, H. Zhu, D. Kim, D. Ma, Y. Xu, J.N. Munday, H.D. Drew, M.S. Fuhrer, L. Hu, Approaching the limits of transparency and conductivity in graphitic materials through lithium intercalation, Nat. Commun. 5 (2014) 4224.
[3] L.L. Zhang, X. Zhao, H. Ji, M.D. Stoller, L. Lai, S. Murali, S. McDonnell, B. Cleveger, R.M. Wallace, R.S. Ruoff, Nitrogen doping of graphene and its effect on quantum capacitance, and a new insight on the enhanced capacitance of N-doped carbon, Energy Environ. Sci. 5 (2012) 9618–9625.
[4] H. Jiang, P.S. Lee, C. Li, 3D carbon based nanostructures for advanced supercapacitors, Energy Environ. Sci. 6 (2013) 41–53.
[5] Z. Jian, V. Raju, Z. Li, Z. Xing, Y.S. Hu, X. Ji, A high-power symmetric Na-ion pseudocapacitor, Adv. Funct. Mater. 25 (2015) 5778–5785.
[6] Y. Zhai, Y. Dou, D. Zhao, P.F. Fulvio, R.T. Mayes, S. Dai, Carbon materials for chemical capacitive energy storage, Adv. Mater. 23 (2011) 4828–4850.
[7] P. Zhang, Z.A. Qiao, Z. Zhang, S. Wan, S. Dai, Mesoporous graphene-like carbon sheet: high-power supercapacitor and outstanding catalyst support, J. Mater. Chem. A 2 (2014) 12262–12269.
[8] Y. Wang, Y. Xia, Recent progress in supercapacitors: from materials design to system construction, Adv. Mater. 25 (2013) 5336–5342.
[9] L.Q. Mai, A. Minhas-Khan, X. Tian, K.M. Hercule, Y.L. Zhao, X. Lin, X. Xu, Synergistic interaction between redox-active electrolyte and binder-free functionalized carbon for ultrahigh supercapacitor performance, Nat. Commun. 4 (2013) 2923.
[10] L.F. Chen, Z.H. Huang, H.W. Liang, Q.F. Guan, S.H. Yu, Bacterial-cellulose-derived carbon nanofiber@MnO_2 and nitrogen-doped carbon nanofiber electrode materials: An asymmetric supercapacitor with high energy and power density, Adv. Mater. 25 (2013) 4746–4752.
[11] P. Simon, Y. Gogotsi, Materials for electrochemical capacitors, Nat. Mater. 7 (2008) 845–854.
[12] Z.S. Wu, D.W. Wang, W. Ren, J. Zhao, G. Zhou, F. Li, H.M. Cheng, Anchoring hydrous RuO_2 on graphene sheets for high-performance electrochemical capacitors, Adv. Funct. Mater. 20 (2010) 3595–3602.
[13] F. Zhang, C. Yuan, J. Zhu, J. Wang, X. Zhang, X.W. Lou, Flexible films derived from electrospun carbon nanofibers incorporated with Co_3O_4 hollow nanoparticles as self-supported electrodes for electrochemical capacitors, Adv. Funct. Mater. 23 (2013) 3909–3915.
[14] J. Yan, Q. Wang, T. Wei, Z. Fan, Recent advances in design and fabrication of electrochemical supercapacitors with high energy densities, Adv. Energy Mater. 4 (2014), http://dx.doi.org/10.1002/aenm.201300816.
[15] H. Jiang, Y. Dai, Y. Hu, W. Chen, C. Li, Nanostructured ternary nanocomposite of rGO/CNTs/MnO_2 for high-rate supercapacitors, ACS Sustain. Chem. Eng. 2 (2014) 70–74.
[16] R. Kötz, M. Carlen, Principles and applications of electrochemical capacitors, Electrochim. Acta 45 (2000) 2483–2498.
[17] K. Wang, Q. Meng, Y. Zhang, Z. Wei, M. Miao, High-performance two-ply yarn supercapacitors based on carbon nanotubes and polyaniline nanowire arrays, Adv. Mater. 25 (2013) 1494–1498.
[18] H.H. Chang, C.K. Chang, Y.C. Tsai, C.S. Liao, Electrochemically synthesized graphene/polypyrrole composites and their use in supercapacitor, Carbon 50 (2012) 2331–2336.
[19] N.S. Choi, Z. Chen, S.A. Freunberger, X. Ji, Y.K. Sun, K. Amine, G. Yushin, L.F. Nazar, J. Cho, P.G. Bruce, Challenges facing lithium batteries and electrical double-layer capacitors, Angew. Chem. Int. Ed. 51 (2012) 9994–10024.
[20] C. Zhang, W. Lv, Y. Tao, Q.H. Yang, Towards superior volumetric performance: design and preparation of novel carbon materials for energy storage, Energy Environ. Sci. 8 (2015) 1390–1403.
[21] Y. Zhu, S. Murali, M.D. Stoller, K.J. Ganesh, W. Cai, P.J. Ferreira, A. Pirkle, R.M. Wallace, K.A. Cychosz, M. Thommes, D. Su, E.A. Stach, R.S. Ruoff, Carbon-based supercapacitors produced by activation of graphene, Science 332 (2011) 1537–1541.
[22] Y. Yang, L. He, C. Tang, P. Hu, X. Hong, M. Yan, Y. Dong, X. Tian, Q. Wei, L. Mai, Improved conductivity and capacitance of interdigital carbon microelectrodes through integration with carbon nanotubes for micro-supercapacitors, Nano Res. 9 (2016) 2510–2519.
[23] J. Liu, L. Zhang, H.B. Wu, J. Lin, Z. Shen, X.W. Lou, High-performance flexible asymmetric supercapacitors based on a new graphene foam/carbon nanotube hybrid film, Energy Environ. Sci. 7 (2014) 3709–3719.
[24] Y. Huang, J. Liang, Y. Chen, An overview of the applications of graphene-based materials in supercapacitors, Small 8 (2012) 1805–1834.
[25] L. Wei, G. Yushin, Nanostructured activated carbons from natural precursors for electrical double layer capacitors, Nano Energy 1 (2012) 552–565.
[26] C. Yin, L. He, Y. Wang, Z. Liu, G. Zhang, K. Zhao, C. Tang, M. Yan, Y. Han, L. Mai, Pyrolyzed carbon with embedded NiO/Ni nanospheres for applications in microelectrodes, RSC Adv. 6 (2016) 43436–43441.
[27] L.F. Chen, Z.Y. Yu, X. Ma, Z.Y. Li, S.H. Yu, In situ hydrothermal growth of ferric oxides on carbon cloth for low-cost and scalable high-energy-density supercapacitors, Nano Energy 9 (2014) 345–354.
[28] L.F. Chen, Z.Y. Yu, J.J. Wang, Q.X. Li, Z.Q. Tan, Y.W. Zhu, S.H. Yu, Metal-like fluorine-doped β-FeOOH nanorods grown on carbon cloth for scalable high-performance supercapacitors, Nano Energy 11 (2015) 119–128.
[29] W. Chen, R.B. Rakhi, M.N. Hedhili, H.N. Alshareef, Shape-controlled porous nanocarbons for high performance supercapacitors, J. Mater. Chem. A 2 (2014) 5236–5243.
[30] K.L. Van Aken, M. Beidaghi, Y. Gogotsi, Formulation of ionic-liquid electrolyte to expand the voltage window of supercapacitors, Angew. Chem. Int. Ed. 54 (2015) 4806–4809.
[31] D. Hulicova-Jurcakova, A.M. Puziy, O.I. Poddubnaya, F. Suárez-García, J.M.D. Tascón, G.Q. Lu, Highly stable performance of supercapacitors from phosphorus-enriched carbons, J. Am. Chem. Soc. 131 (2009) 5026–5027.
[32] G. Xu, B. Ding, J. Pan, J. Han, P. Nie, Y. Zhu, Q. Sheng, H. Dou, Porous nitrogen and phosphorus co-doped carbon nanofiber networks for high performance electrical double layer capacitors, J. Mater. Chem. A 3 (2015) 23268–23273.
[33] L.L. Zhang, X.S. Zhao, Carbon-based materials as supercapacitor electrodes, Chem. Soc. Rev. 38 (2009) 2520–2531.
[34] A. González, E. Goikolea, J.A. Barrena, R. Mysyk, Review on supercapacitors: technologies and materials, Renew. Sust. Energy Rev. 58 (2016) 1189–1206.
[35] G. Wang, L. Zhang, J. Zhang, A review of electrode materials for electrochemical supercapacitors, Chem. Soc. Rev. 41 (2012) 797–828.
[36] X. Li, B. Wei, Supercapacitors based on nanostructured carbon, Nano Energy 2 (2013) 159–173.
[37] G. Xu, J. Han, B. Ding, P. Nie, J. Pan, H. Dou, H. Li, X. Zhang, Biomass-derived porous carbon materials with sulfur and nitrogen dual-doping for energy storage, Green Chem. 17 (2015) 1668–1674.
[38] T. Lin, I.W. Chen, F. Liu, C. Yang, H. Bi, F. Xu, F. Huang, Nitrogen-doped mesoporous carbon of extraordinary capacitance for electrochemical energy storage, Science 350 (2015) 1508–1513.
[39] Y. Deng, Y. Xie, K. Zou, X. Ji, Review on recent advances in nitrogen-doped carbons: preparations and applications in supercapacitors, J. Mater. Chem. A 4 (2016) 1144–1173.
[40] W.H. Lee, J.H. Moon, Monodispersed N-doped carbon nanospheres for supercapacitor application, ACS Appl. Mater. Interfaces 6 (2014) 13968–13976.
[41] G. Xu, B. Ding, P. Nie, L. Shen, J. Wang, X. Zhang, Porous nitrogen-doped carbon nanotubes derived from tubular polypyrrole for energy-storage applications, Chem. Eur. J. 19 (2013) 12306–12312.
[42] L. Qie, W.M. Chen, Z.H. Wang, Q.G. Shao, X. Li, L.X. Yuan, X.L. Hu, W.X. Zhang, Y. H. Huang, Nitrogen-doped porous carbon nanofiber webs as anodes for lithium ion batteries with a superhigh capacity and rate capability, Adv. Mater. 24 (2012) 2047–2050.
[43] Z. Wen, X. Wang, S. Mao, Z. Bo, H. Kim, S. Cui, G. Lu, X. Feng, J. Chen, Crumpled nitrogen-doped graphene nanosheets with ultrahigh pore volume for high-performance supercapacitor, Adv. Mater. 24 (2012) 5610–5616.
[44] J. Wei, D. Zhou, Z. Sun, Y. Deng, Y. Xia, D. Zhao, A controllable synthesis of rich nitrogen-doped ordered mesoporous carbon for CO_2 capture and supercapacitors, Adv. Funct. Mater. 23 (2013) 2322–2328.
[45] J.W.F. To, Z. Chen, H. Yao, J. He, K. Kim, H.H. Chou, L. Pan, J. Wilcox, Y. Cui, Z. Bao, Ultrahigh surface area three-dimensional porous graphitic carbon from conjugated polymeric molecular framework, ACS Cent. Sci. 1 (2015) 68–76.
[46] J. Tang, R.R. Salunkhe, J. Liu, N.L. Torad, M. Imura, S. Furukawa, Y. Yamauchi, Thermal conversion of core-shell metal-organic frameworks: a new method for selectively functionalized nanoporous hybrid carbon, J. Am. Chem. Soc. 137 (2015) 1572–1580.
[47] F. Meng, X. Zhang, R. Li, J. Zhao, X. Xuan, X. Wang, J. Zou, Q. Li, Electro-induced mechanical and thermal responses of carbon nanotube fibers, Adv. Mater. 26 (2014) 2480–2485.
[48] G. Xu, J. Yuan, X. Tao, B. Ding, H. Dou, X. Yan, Y. Xiao, X. Zhang, Absorption mechanism of carbon-nanotube paper titanium dioxide as a multifunctional barrier material for lithium-sulfur batteries, Nano Res. 8 (2015) 3066–3074.

[49] L. Pan, G. Yu, D. Zhai, H.R. Lee, W. Zhao, N. Liu, H. Wang, B.C.K. Tee, Y. Shi, Y. Cui, Z. Bao, Hierarchical nanostructured conducting polymer hydrogel with high electrochemical activity, Proc. Natl. Acad. Sci. 109 (2012) 9287–9292.
[50] J. Han, G. Xu, H. Dou, D.R. MacFarlane, Porous nitrogen-doped carbon microspheres derived from microporous polymeric organic frameworks for high performance electric double-layer capacitors, Chem. Eur. J. 21 (2015), http://dx.doi.org/10.1002/chem.201580661.
[51] J. Xu, K. Wang, S.Z. Zu, B.H. Han, Z. Wei, Hierarchical nanocomposites of polyaniline nanowire arrays on graphene oxide sheets with synergistic effect for energy storage, ACS Nano 4 (2010) 5019–5026.
[52] S. Stankovich, D.A. Dikin, R.D. Piner, K.A. Kohlhaas, A. Kleinhammes, Y. Jia, Y. Wu, S.T. Nguyen, R.S. Ruoff, Synthesis of graphene-based nanosheets via chemical reduction of exfoliated graphite oxide, Carbon 45 (2007) 1558–1565.
[53] Y. Xu, K. Sheng, C. Li, G. Shi, Self-assembled graphene hydrogel via a one-step hydrothermal process, ACS Nano 4 (2010) 4324–4330.
[54] H. Gao, L. Song, W. Guo, L. Huang, D. Yang, F. Wang, Y. Zuo, X. Fan, Z. Liu, W. Gao, R. Vajtai, K. Hackenberg, P.M. Ajayan, A simple method to synthesize continuous large area nitrogen-doped graphene, Carbon 50 (2012) 4476–4482.